Soft Matter

PAPER

View Article Online
View Journal | View Issue

Cite this: *Soft Matter*, 2017, 13, 7793

Ion transport mechanisms in lamellar phases of salt-doped PS–PEO block copolymer electrolytes†

Vaidyanathan Sethuraman, Santosh Mogurampelly and Venkat Ganesan *

We use a multiscale simulation strategy to elucidate, at an atomistic level, the mechanisms underlying ion transport in the lamellar phase of polystyrene–polyethylene oxide (PS–PEO) block copolymer (BCP) electrolytes doped with $LiPF_6$ salts. Explicitly, we compare the results obtained for ion transport in the microphase separated block copolymer melts to those for salt-doped PEO homopolymer melts. In addition, we also present results for dynamics of the ions individually in the PEO and PS domains of the BCP melt, and locally as a function of the distance from the lamellar interfaces. When compared to the PEO homopolymer melt, ions were found to exhibit slower dynamics in both the block copolymer (overall) and in the PEO phase of the BCP melt. Such results are shown to arise from the effects of slower polymer segmental dynamics in the BCP melt and the coordination characteristics of the ions. Polymer backbone-ion residence times analyzed as a function of distance from the interface indicate that ions have a larger residence time near the interface compared to that near the bulk of lamella, and demonstrates the influence of the glassy PS blocks and microphase segregation on the ion transport properties. Ion transport mechanisms in BCP melts reveal that there exist five distinct mechanisms for ion transport along the backbone of the chain and exhibit qualitative differences from the behavior in homopolymer melts. We also present results as a function of salt concentration which show that the mean-squared displacements of the ions decrease with increasing salt concentration, and that the ion residence times near the polymer backbone increase with increasing salt concentration.

Received 6th July 2017,
Accepted 10th October 2017

DOI: 10.1039/c7sm01345k

rsc.li/soft-matter-journal

1 Introduction

There has been a surge in the number of studies examining the properties of solid polymer electrolytes (SPEs) as membranes for lithium ions batteries.[1–11] While many of the investigations have been concerned with homopolymer electrolytes,[5,7,12–15] such materials suffer from the disadvantage that properties like conductivity and mechanical strength are often inversely correlated, and hence cannot be manipulated independently.[7,13] To overcome such a limitation, multicomponent polymers such as block copolymers[16,17] and polymer blends,[18,19] which enable access to multifunctionality have been proposed as alternative SPEs.[9,20–23]

In the above pursuit of multifunctional electrolytes, self-assembled block copolymers (BCP) consisting of alternating conducting and non-conducting block(s) have emerged as especially attractive candidates.[9,20,21,23–28] In the case of BCP electrolytes, the conducting blocks, which possess a lower glass transition temperature (T_g), act as the ion conducting pathways, whereas the nonconducting blocks, which typically possess a higher T_g, serves to provide the mechanical strength.[9,20] A number of experiments in this regard have demonstrated that the conductivity of ions in such systems depend both on the morphology and the underlying chemistry of the conducting/nonconducting blocks.[22,29,30] Further, recent studies have demonstrated that ionic conductivity in block copolymers exhibit non-trivial salt concentration dependencies.[22,27]

A number of past studies have examined the mechanisms of ion transport in homopolymer electrolytes such as PEO.[31–39] Ion transport in such electrolytes has been demonstrated to occur primarily by the motion of ions along the polymer backbone, referred to commonly as "hopping motion."[33,34] Computer simulations by Borodin *et al.*,[33,40] and Heuer *et al.*,[38] have demonstrated that there primarily exist two types of hopping: (i) intramolecular hopping in which the ions hop along one chain; and (ii) intermolecular hopping wherein the ions hop between chains. Further, it was shown that the hopping rates are themselves intrinsically tied to the polymer segmental dynamics.

Despite significant experimental advances in the context of BCP electrolytes, a level of understanding of ion-transport mechanisms in BCP systems comparable to homopolymers does not exist. Coarse-grained simulations of the ion transport in BCPs have shown that there exists a spatial heterogeneity in the polymer segmental dynamics whose length scale is controlled

Department of Chemical Engineering, University of Texas at Austin, Austin, Texas 78712, USA. E-mail: venkat@che.utexas.edu

† Electronic supplementary information (ESI) available. See DOI: 10.1039/c7sm01345k

by the interfacial width of the polymer.[28,41,42] Such heterogeneities have been argued to influence the MW dependence of conductivity of diblock and tapered copolymers.[41–43] Although, such insights have proven informative, detailed atomistic level studies ion transport mechanism and its relation with the morphology and structure of the BCP are still lacking. Some unresolved questions in this regard include,

1. Do ion motions in BCPs exhibit spatially heterogeneous dynamics arising as a consequence of microphase separation?

2. Is the segmental dynamics of the conducting block influenced by the microphase separation, and do such effects influence the ion dynamics?

3. How are the mechanisms of ion motion influenced by microphase separation?

4. What is the influence of salt concentration on the above-mentioned features?

Atomistic simulations of microphase separated BCPs have been largely hindered by the significant computational times involved in generating equilibrated configurations of ion-doped self-assembled BCP morphologies.[44–46] To overcome such a challenge, in a recent work,[47] we presented a multiscale simulation strategy to generate equilibrium microphase segregated morphology at atomistic level. Our recent article[47] identified the influence of microphase segregation on the equilibrium structural coordination between ions and polymers. Therein, it was shown that microphase segregation leads to stronger ion–ion and ion–oxygen backbone coordination. Further, a heterogeneity in strength of coordination between ion and atom pairs was observed as a function of distance from the lamellar interface for microphase segregated BCPs.

Motivated by the lack of understanding on ion transport mechanisms in microphase segregated BCPs, in this study, we adapted our multiscale simulation approach[47] to elucidate the ion transport mechanisms at an atomistic level in such systems. We compared such results with those observed in pure homopolymer melts, and also characterized the influence of salt concentrations. The results arising from such a study are reported in this article.

The rest of the article is organized as follows. Details of the simulation methodology and the different measures which are used to quantify the ion transport characteristics are presented in Section 2. In Section 3.1, the results obtained for global and local ion dynamics such as mean squared displacement and the residence time correlation of ions are compared with those obtained in the context of homopolymer melts. The mechanisms underlying ion transport in BCPs are discussed in Section 3.2. The effect of salt loading upon ion dynamics and the transport mechanisms are presented in Section 3.3. Finally, our findings are summarized in Section 4.

2 Simulation details

In an earlier article,[47] we presented a detailed exposition of the multiscale simulation technique that was employed to generate lamellar phases of ion-doped block copolymers at an atomistic level of resolution. The simulation methodology and parameters chosen for the present work are identical to our earlier work and we refer reader to ref. 47 for more details. For completeness, we present here a short summary of the underlying ideas and elaborate on the details of the force fields in the Section S1 of ESI.†

The simulation methodology consists of three major steps: (i) performing atomistic simulations on PS–PEO block copolymer melt (without ions) at high temperature (600 K) using TraPPE force fields[48–50] to extract the intramolecular interaction parameters for use in coarse-grained simulations;[44,51] (ii) performing single chain in mean field (SCMF)[52–56] coarse-grained simulations on diblock copolymer melts using the intramolecular interaction parameters obtained from step (i) to generate the ordered phases of block copolymers; (iii) reintroduction of atomistic details of PS and PEO blocks and the salt ($LiPF_6$) into the microphase separated morphology.[47,51,57–59] Subsequently the atomistic morphology is subjected to a long *NPT* run (40–120 ns) for equilibration and analysis of ion transport properties and mechanisms.

In all the simulations, the number of chains for the BCP were fixed at 700 chains. Each chain consisted of 151 UA beads with 10 PS and 23 PEO monomeric units corresponding to a 50 : 50 composition of block copolymer. Three different cases of salt concentration were studied with the ratio between the number of ether oxygen monomers (EO) to lithium ions (EO : Li) fixed at 10 : 1, 20 : 1 and 30 : 1 respectively. All the simulations were carried out at a temperature of 350 K. For comparison to BCPs, pure PEO homopolymer melts were also simulated at 350 K. For the latter, *NPT* simulation was performed on the ion–polymer system starting from random initial conditions. For comparison with the same MW PEO block, we chose PEO homopolymers consisting of 23 monomeric units. All the simulations were performed using LAMMPS.[60]

Motivated by computational efficacy, in this work we use non-polarizable force fields as opposed to the many body force fields utilized by Borodin and coworkers. The issue of the differences in dynamical characteristics predicted by polarizable *versus* non-polarizable force fields has been discussed in a few earlier works.[33,61] In general, the dynamical characteristics predicted by non-polarizable force fields are slower than those arising in simulations including polarizable force fields. While it is not clear if there is a single physical reason which can be attributed to such trends, more often than not, polarizable force fields, which are multibody in nature, predict weaker coordination characteristics for the anions and cations. Consistent with such trends, the ion–EO coordination is stronger in our simulations (non-polarizable force fields) compared to those reported by Borodin and coworkers.[62] Explicitly, the maximum value in the ion–EO coordination for many body polarizable force fields[62] is 17 whereas in our case the maximum value is 24. Such stronger coordination implies that the ion motion is more restricted by the motion of the polymer segments, which by themselves are intrinsically slower, leading to a slower diffusion for non-polarizable force fields. Moreover, the dielectric constant predicted by our force field for PEO was 4.71, whereas, the experimental values have been reported closer to 7.0.[47] Such a lower dielectric constant leads to stronger

coordination between the anion and cation and thereby hinders the diffusion of the ions.

Further, we note that our simulations are effected at a low temperature of 350 K to maintain the phase segregation of the BCP at the low MWs. Due to the preceding factors, for many of the results reported, the true long-time limit of trends are not manifested. However, despite this limitation, the influence of microphase segregation and salt concentration is evident within the time span of our simulations, and constitutes the basis of our discussion and understanding.

A number of different measures were used to quantify the dynamics of the ions and transport mechanisms of the ions both, spatially locally, and averaged over the entire lamellar domain. We discuss them below.

2.1 Mean squared displacements

The mobility of the ions and atoms were quantified using the mean squared displacement (MSD) of the monomers defined as:

$$\left\langle \mathbf{r}^2 \right\rangle = \sum_{i=0}^{N} \left\langle (\mathbf{r}_i(t) - \mathbf{r}_i(0))^2 \right\rangle \tag{1}$$

where $\mathbf{r}_i(t)$ denotes the position of the ith monomer at time t and, $\langle\rangle$ denotes an ensemble average.

2.2 Residence time correlation function

Ion transport in homopolymers has been shown to occur *via* ion hopping along the backbone of the conducting polymer. To characterize such transport, we quantified the ion–ether oxygen residence time, which is defined as the average time of coordination between the Li^+ cations and the oxygen atoms (referred to as "ether oxygens" in subsequent discussion). To compute such a quantity, we consider a residence time function ($H(t)$), which is assigned a value of unity if a lithium ion is found within the first coordination shell (r_c = 2.4 Å) of an oxygen atom or else it is assigned a value of zero:

$$H(t) = \begin{cases} 1, & \text{if } r \le r_c \\ 0, & \text{if } r > r_c \end{cases}$$

Subsequently, a normalized residence time autocorrelation function is obtained using:

$$A(t) = \frac{\langle H(t)H(0)\rangle}{\langle H(0)^2\rangle}. \tag{2}$$

To compute the average residence time (τ_r), the above correlation function is fitted to a stretched exponential curve of the form: $A\exp(-(t/\tau)^{\beta})$, where τ and β are fitting constants, and then, τ_r is calculated using $\tau_r = \tau\Gamma(1 + 1/\beta)$, where $\Gamma(n)$ represents the Gamma function.

2.3 Polymer dynamics

As discussed in the Introduction, ion transport in polymer electrolytes is believed to be tightly correlated with the dynamics of polymer segments. In this work, we consider the normalized dihedral–dihedral autocorrelation function ($C_{\phi\phi}$) to quantify the polymer segmental dynamics.

$$C_{\phi\phi} = \frac{\langle \cos(\phi(t))\cos(\phi(0))\rangle - \langle\cos(\phi(0))\rangle^2}{\langle \cos(\phi(0))\cos(\phi(0))\rangle - \langle\cos(\phi(0))\rangle^2} \tag{3}$$

where $\phi(t)$ denotes the dihedral angle of the polymer backbone. The results presented in this work correspond to the autocorrelation of CCOC dihedrals along the polymer backbone. Similar to the residence time autocorrelation function described earlier, the dihedral autocorrelation is fitted to a stretched exponential curve to extract the average segmental relaxation time, τ_ϕ.

2.4 Local dynamical characteristics

The local dynamic properties of the ions in the microphase separated BCP were analyzed as a function of the distance ($|z - z_i|$) from the interface, where z_i represents the location of the interface of the lamella and z denotes the distance in the plane normal to the interface. Interfacial positions are calculated from the PS–PEO density profiles as those locations obeying $\rho_{PS}(z) = \rho_{PEO}(z)$ (ρ_i corresponds to the normalized density of the ith component).

For the analysis of local dynamics, three separate regions of equal volume were defined: (i) "Near the interface" as defined by the region $\{0 \le |z - z_i| \le 0.05D\}$; (ii) In the "bulk of the domain" defined as $\{0.30D \le |z - z_i| \le 0.35D\}$; and (iii) "Between the bulk and interface" defined as $\{0.15 \le |z - z_i| \le 0.20D\}$, where D represents the average domain width. Subsequent to defining the regions of interest, the ions that are in each domain at t = 0 are identified. The dynamic property of the particular layer is then obtained as an ensemble average of the property of the ions that are present in the corresponding layer at t = 0. We present the results obtained individually in the PEO and PS domains along with those averaged over both the domains.

2.5 Ion–chain coordination

An important equilibrium feature for characterizing the mechanism of ion transport is the average number of chains to which an ion is coordinated. Ions coordinated with multiple chains during the course of simulation are expected to have slower mobilities compared to those coordinated with a single chain.[15,33] To quantify such characteristics, we compute the distribution of ions which are coordinated to single and multiple chains using a function $F(n)$ representing the fraction of ions which are coordinated with n number of chains and is defined as:

$$F(n) = \frac{N_{Li}(n)}{N_{Li}^{t}} \tag{4}$$

where $N_{Li}(n)$ and $N_{Li}^{t}(n)$ represent the number of ions coordinated with n chains and total number of ions. A chain is said to be coordinated with a given lithium atom, if at least one oxygen atom of the chain under consideration lies within the first coordination shell ($r <$ 2.4 Å) of the given lithium atom.

3 Results and discussion

3.1 Ion dynamics in block copolymers

In this section, we present results comparing the ion transport characteristics in the lamellar phase of PS–PEO block copolymers with those in the pure PEO homopolymer.

Fig. 1(a) compares the mean squared displacement (MSD) of lithium ions in homopolymers and block copolymers (averaged over PEO and PS domains) for a salt concentration of EO : Li = 20 : 1. In Fig. 1(b) we compare the mean squared displacements of ions located respectively in PS and PEO domains to the homopolymer PEO melt. For block copolymers, the MSDs represent dynamics averaged in the directions parallel to the lamellar plane, whereas for the homopolymers, MSDs are averaged in all three spatial directions. In contrast to the previous studies on homopolymers which reported ion diffusivity values,[40] in this study, we are limited by the statistics at low temperatures, and are unable to extract the long-time diffusivities. However, by comparing mean squared displacements of homopolymer and BCPs, a qualitative picture of the effect of microphase segregation on ionic diffusivities can nevertheless be identified.

Three observations emerge from Fig. 1(a) and (b):

(i) The MSDs of Li^+ in PS domains are seen to be smaller in magnitude as that of those in the PEO domain of the BCP (Fig. 1(b)). The MSDs of PF_6^- counterions follow similar trends and are displayed in Fig. S1(a) of ESI.† To rationalize this observation, we note that the nonconducting PS block has a higher T_g ($\approx$380 K)[63] compared to that of PEO ($T_g \approx 210$ K)[64] and is hence expected to have slower dynamics. Such slower polymer dynamics is expected to lead to slower ion dynamics in the PS phase;

(ii) In both the block copolymers and homopolymers, the counterions (PF_6^-) are seen to diffuse faster compared to that of the ions (Li^+) themselves (Fig. 1(a)). Such a trend in relative mobilities of anions and cations is consistent with earlier observations in the context of homopolymers.[33] More pertinently, the anions are also seen to move slower in BCPs compared to HPs. The coordination between lithium and PF_6^- counterions[47] coupled with the slower dynamics of Li^+ ions themselves in BCPs (see (iii) below) can be expected to serve as an additional factors which hinder the dynamics of the anions in BCPs;

(iii) Most interestingly, the lithium ions are observed to diffuse slower (Fig. 1(a)) in the block copolymer compared to that in the homopolymer. The fact that the MSDs in the PEO homopolymer melt are larger than those in the PEO domains of BCPs (Fig. 1(b)) demonstrates that such trends are not a result of the slow dynamics in PS phase, but instead arise as a consequence of the inherent ion dynamics in the PEO phase of the block copolymers. Such results are broadly consistent with previous experimental observations[20] and coarse-grained simulations.[42]

To understand the origins of (iii), we note that a number of previous studies have demonstrated that ion transport in polymer electrolytes to be intrinsically linked to the polymer segmental dynamics.[40] Additionally, prior work[41,42] (from coarse-grained simulations) has shown that as a consequence of the

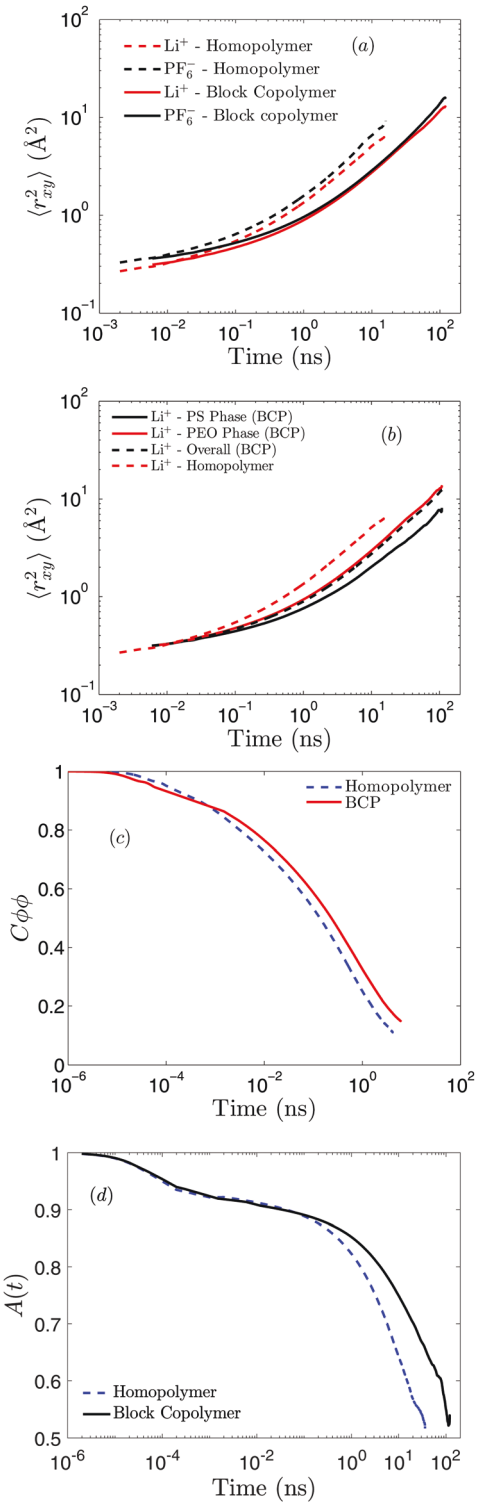

Fig. 1 (a) A comparison of the time dependence of ion (Li^+) and counter-ion (PF_6^-) mean-squared displacements in pure PEO melt and block copolymers. Only the portion beyond the initial ballistic regime is depicted; (b) a comparison of the time dependence of mean squared displacements of ions in PS and PEO domains of the BCP with that in pure PEO melt (for the depiction in linear scale see Fig. S1(b), ESI†). Only the portion beyond the initial ballistic regime is depicted; (c) polymer segmental dihedral–dihedral autocorrelation functions; (d) normalized residence time auto-correlation function in homopolymers and block copolymers.

covalent linking of the more mobile conducting block (PEO) to the slower block (PS) and the accompanying microphase separation, the dynamics of EO segments become hindered in the interfacial regions of the BCP lamella. Such a factor has been argued in prior studies[10,27,28,42,43] to be responsible for the lower ion mobilities in BCP systems relative to the homopolymers.

To probe the validity of the above arguments in the context of our simulation configurations, in Fig. 1(c), we compare the relaxation of polymer dihedral autocorrelation function, $C_{\phi\phi}$ in the PEO phase of the block copolymer melt with those in the pure PEO homopolymer melt. From the results therein, it can be seen that the dihedral autocorrelation for the PEO phase of the BCP indeed decays slower than that in the pure PEO melt. More explicitly, fitting a stretched exponential function yields a dihedral relaxation time (τ_ϕ) as 2.4 ns for pure PEO melt and 5.4 ns for the PEO phase in the BCP melt. Such results demonstrate polymer dynamics is indeed slower in the conductive phase in the BCP melt compared to the pure PEO homopolymer melt.

How/why does the slower polymer dynamics influence ion motion? Previous studies[40] have shown that ion motion in salt-doped polymer electrolytes such as PEO involves successive hops of the cations along the polymer backbone with a time scale strongly correlated to the segmental relaxation times of the polymer. To demonstrate such a correlation for our system, we consider the lithium ion–ether oxygen residence times, which quantifies the time over which the Li^+ cations are bound to the ether oxygen atom. Such residence times have been shown related directly to the time between successive ion hops, and quantifies in a direct manner the correlation between ion and polymer segmental dynamics.

Fig. 1(d) compares the normalized residence time autocorrelation function (ACF, eqn (2)) for the BCP system with the corresponding results in pure homopolymer melts. Therein, it is clearly seen that the decay of such correlation functions is correspondingly much slower in BCP compared to the homopolymer. More explicitly, if we crudely fit the relaxation to a stretched exponential (despite the fact that ACF has not decayed sufficiently), we find that such time constant for the pure PEO melt and the BCP melt are 0.804 μs and 1.415 μs respectively (a representative fit is shown in Fig. S2, ESI†), which confirms the order of magnitude slower dynamics of ions in BCPs (we note that the residence times obtained in our simulations are of the order of hundreds of nanoseconds for pure homopolymer melt in contrast to the results of the order of 10–50 ns obtained by Borodin *et al.*[33] Such differences arise as a consequence of not using any polarization interactions or charge scaling to accelerate the dynamics of the system).

Together, the results of Fig. 1(c) and (d) provide evidence that the slower ion dynamics in BCPs arises in turn from the slower polymer segmental dynamics and its influence on the time scale for ion hopping along the polymer backbone. As discussed above, such effects on the polymer segmental dynamics of EO segments have been argued to arise as a consequence of the covalent linking of the more mobile conducting block (PEO) to the slower block (PS) and the interfacial effects accompanying microphase separation.[10,27,28,42,43] To provide direct evidence for

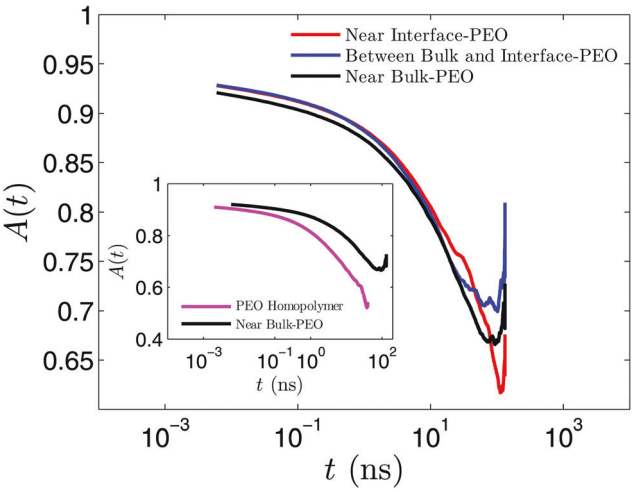

Fig. 2 Residence time autocorrelation functions as a function of time for different layers as a function of distance from interface. Only the portion of the residence time autocorrelation function beyond the initial decay is depicted.

such a mechanism, in Fig. 2 we display the spatial variation of ion residence correlation functions and the residence times in the PEO phase of the block copolymer melt (for EO : Li = 30 : 1) as a function of the distance from the interface. Explicitly, it is seen that the residence time correlation function decays slower near the interface relative to the bulk of the PEO phase in the BCP. Interestingly, we observe that the decay of the correlation function in the bulk of the PEO phase is still slower than that of the pure homopolymer melt. Such a result arises from the fact that the MW of the block copolymer considered in our simulations is small and the microphases correspond to moderate segregation regime. Thus, the interfacial effects arising from the glassy PS blocks and microphase separation are expected to be extend to the bulk of the PEO phase in the BCP.

Together, the results displayed in Fig. 1(a)–(d) and 2 demonstrate a consistent picture of ion dynamics in microphase separated block copolymers and the differences from the corresponding homopolymer systems. Explicitly, the covalent linking of the PEO blocks to the PS blocks and the accompanying microphase separation is seen to slow the dynamics of EO segments in BCP phases. Such an effect is seen to directly influence ion–EO residence times underlying the hopping dynamics of the cations and the accompanying ion mobilities in BCP phases.

In concluding this section, we raise the question whether the effects noted in BCPs arise exclusively from the combined influence of the glassier PS block and microphase separation upon PEO segmental dynamics. To address this issue, we recall the results from our previous work on the equilibrium characteristics of ion-doped BCP melts (Fig. 3(a)) which showed that the binding of the cations with ether oxygens are stronger in BCP melt compared to that in homopolymer melt. Such results were demonstrated to arise from the stronger binding in the PS phase of the BCP melt where there is only fewer number of ether oxygens for the binding of cations. Such a stronger binding of

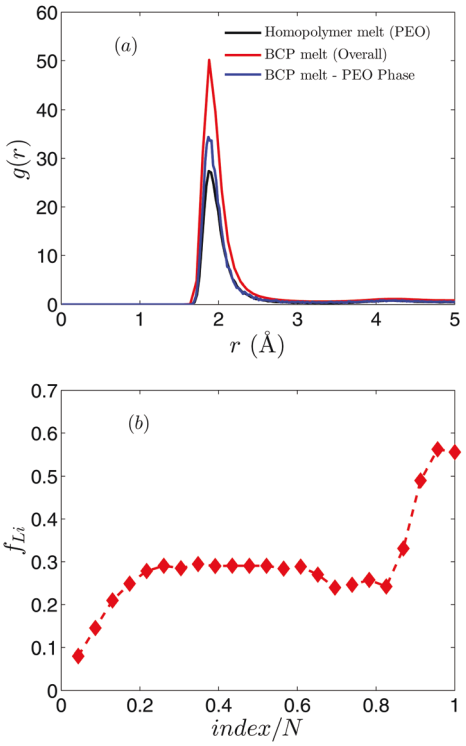

Fig. 3 (a) Comparison of Li–O RDF in BCP melt, PEO phase of BCP melt and pure PEO melt; (b) fraction of ions distributed as a function of the oxygen index in BCP. Both the figures are adapted with permission from Sethuraman *et al.* (Fig. 6 and 7 of original article).[47]

ions with the backbone is also expected to contribute to a slower polymer dynamics and larger ion residence times. Similarly, in our previous work,[47] it was shown that the number of oxygen atoms that surround lithium atoms is more near the bulk of the PEO phase when compared to those near the PS–PEO interface (reproduced in Fig. 3(b)). Such a higher density of oxygens near the bulk endows a higher propensity for the lithium ions to move to the neighboring oxygen atoms, thus causing lower residence times in the bulk of PEO domains. Such results suggest that the dynamics of the ions are also likely to be influenced by the changes in equilibrium coordination characteristics arising from microphase separation in addition to changes in the PEO segmental dynamics. Unfortunately, in realistic simulations such as those pursued in our study, it is not possible to decouple the effects arising from such equilibrium coordination behavior and the dynamical asymmetry inherent in the blocks.

3.2 Ion transport mechanisms in block copolymers

The preceding section presented results for the local and global dynamics of ions in block copolymers as quantified through the mean-squared displacements and residence time correlations. In this section, we present results which provide insights into whether the modes of ion transport are themselves influenced by the microphase separation of the BCP.

To quantify different modes of ion transport in BCPs, we adopt the methodology used by Borodin *et al.*,[33] for homopolymers. Explicitly, during the simulations, a fraction (chosen as 10% in our study) of the entire lithium ions are screened for the presence of an oxygen atom (or anions) in its first coordination shell every 6 ps. Such a fraction corresponds to 30–161 lithium atoms for the case of block copolymer salt ratios under consideration. An oxygen atom or PF_6^- anion is said to be in the vicinity of a lithium ion if such atoms are within the first coordination shell of the lithium ion for a period of atleast 30 ps every 60 ps window. The oxygen atoms of every chain to which a particular lithium ion is coordinated are then characterized as a function of time to identify the different modes of ion transport and hopping.

Fig. 4 displays the different modes of ion transport that were observed in our block copolymer system in a representation that depicts the oxygen segments corresponding to different chains with different colors and contiguous ether oxygens separated by solid lines. To maintain clarity, data only every 60 ps are shown in Fig. 4. For ease of understanding, a schematic representation of various ion transport mechanisms is also shown alongside the corresponding results. Overall, five distinct mechanisms for ion hopping along the backbone of the chain were observed in the case of block copolymers.

- Type 1: Fig. 4(a) displays an intramolecular transport mechanism wherein only one chain is involved in the transport of that particular ion (shown by blue color). Further, a solid line separates two contiguous sets of oxygen atoms (first oxygen set having indices between 10 and 16 and second oxygen set having indices between 19 and 23). In this case, the ions are within the coordination shell of the oxygen atoms of the same chain for the entire period of the simulation window. At short time scales ($t < t_1 \approx 20$ ns), the ion is complexed with only 4 of the contiguous oxygen segments (segments 23 and 11–14). The combined motion of the chain ends and the ions themselves change the complexation of ions from 4 oxygen segments to 6 segments of the same chain for $t > t_1$ (segments 20–23 and 14–16). Such a hopping is pictorially represented on the right side of the plot. Such results have also been observed in the context of PEO HPs wherein the ions hopped along the same chain for the entire period of simulation.[33]

- Type 2: Fig. 4(b) displays the mode wherein the ions are coordinated with the same two chains for the entire course of the simulation. In our analysis, a significant number of ions are linked to at least two chains during the course of our simulations. Two distinct classes of motion were observed within this context. (i) The ions "hopped" along the backbone, *i.e.*, the oxygen segment to which the ions are coordinated changed over the simulation time as shown in Fig. 4(b); (ii) the ions were coordinated to two chains, but were linked to the same set of oxygen segments for the entire duration of simulation (see Fig. S3 of ESI†). Again, in the context of homopolymers, similar ion transport mechanism wherein the ions are coordinated to two separate chains were observed.[33]

- Type 3: Fig. 4(c) displays the case wherein the ions are initially coordinated with a single chain until about 25 ns ($t < t_1$), subsequent to which the ions become complexed by multiple chains for the rest of the simulation. Such mechanisms were also observed in the context of our homopolymer systems.

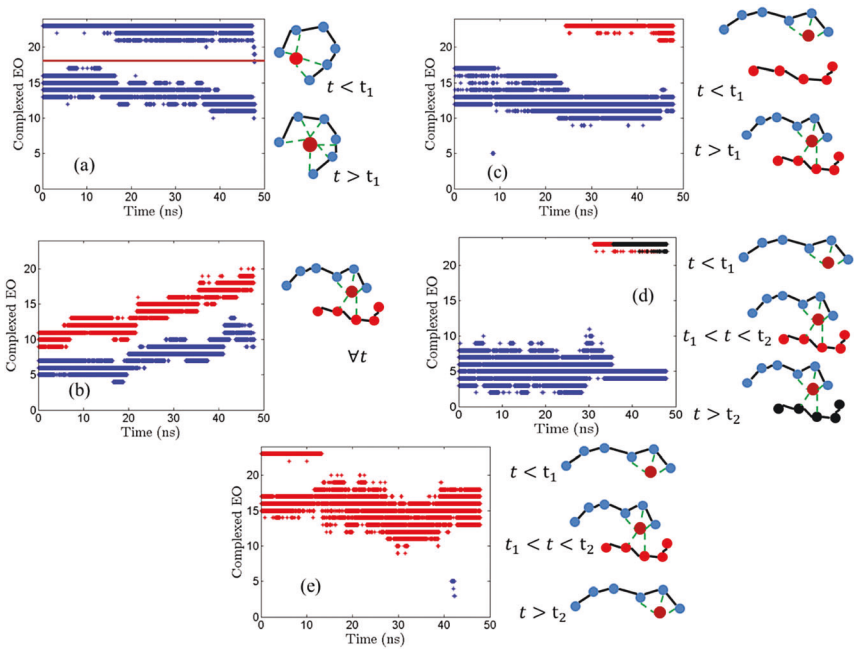

Fig. 4 (a) Intramolecular hopping; (b) hopping along two chains; (c) hopping along chain one and switching to chain two while continuing its attachment with chain one; (d) hopping to chains two and three while keeping its initial attachment with chain one; (e) transient hopping to chain two and back to chain one. The figures to the right of the plot are cartoons depicting the respective mechanism. The oxygen segments corresponding to different chains are displayed using different colors and contiguous ether oxygens are separated by solid lines.

However, in the case of homopolymers, the number of such events were smaller compared to those in BCP melts. Such results indicate that the conformational arrangement of the chains in the lamellar microphases facilitate enhanced transitions from single chain to multiple chain based hopping mechanism. Such conclusions are also supported by results presented in Fig. 5(b) and (c) below.

• Type 4: Fig. 4(d) displays a case wherein the ions are linked to one chain until $t = t_1 = 30$ ns. Subsequently, for a short time ($t_1 < t < t_2 = 35$ ns), ions are linked to the end segments of a different chain. However, such coordination is short lived and the ions hop on to a different chain. Here the chain ends are found to play an important role in the intersegmental hop of ions, and was found to occur (relatively) more often than homopolymers due to the proximity of different chain ends in the lamellar phase.

• Type 5: Fig. 4(e) displays the case wherein the ions are connected with a single chain for most of the course of simulation. However, for a very small fraction of time, transient coordinations with ($t \approx 42$ ns) other chains were also observed. In both BCPs and HPs we observed that occurrences of such cases are very rare.

While the results of Fig. 4 presented the detailed ion transport mechanism in BCP melts and indicated qualitative similarities to the behavior in homopolymers, in Fig. 5, we quantify such ion hops and compare the trends in BCPs with homopolymers.

In Fig. 5a, we present the fraction of ions (with respect to the total ions in the system) that are coordinated with different number of chains over the time period of simulation (a logarithmic representation of the plots is given in Fig. S4, ESI† to depict the smaller values more clearly). It can be seen that in both homopolymers and block copolymers, the majority of the ions are attached to either one or two chains. More interestingly, the almost quantitative agreement between HPs and BCPs indicate that microphase segregation does not change the average coordination behavior of the ions with the chains at this salt concentration. Previous works on homopolymer melts demonstrated that ions which are coordinated to one chain move faster compared to those coordinated with multiple chains.[33] Our results above lend support to the hypothesis that the difference in mobility of ions between HPs and BCPs do not arise from the differences in coordination of atoms with multiple chains, but by the inherently slower polymer segmental dynamics in the BCP itself as discussed in the previous section.

Fig. 5(b) and (c) compares the coordination behaviors of HPs and BCPs based on the average of the instantaneous number of chains ($\hat{C}(n)$) an ion is coordinated. In this representation, if an ion is coordinated with 2 chains for a small period of time followed by 3 chains for the rest of the simulation, the average chain coordination will be a value between 2 and 3. In contrast, an ion which is coordinated with only one chain throughout the simulation will have a value of 1. Thus, non-integer values correspond to changes in the instantaneous number of coordination. Note that, such an analysis is different from that presented in the context of Fig. 5(a) wherein only the ensemble average of the fraction of ions coordinated with multiple chains are displayed.

The following observations emerge from Fig. 5(b) and (c): (i) In both BCPs and homopolymer melts, ions which are bound to one/two chains are seen to persist in their coordination state for most of the time scale of simulation, suggesting that events

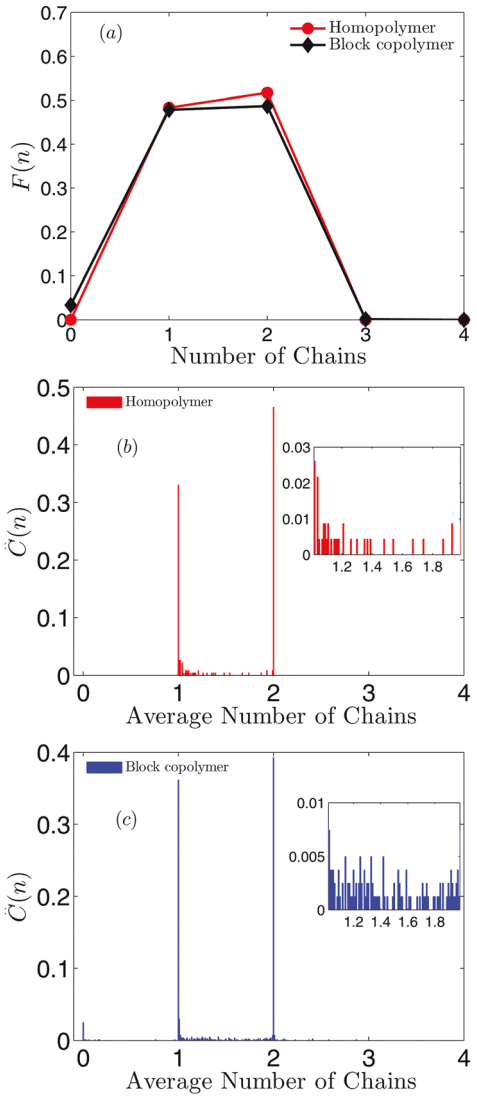

Fig. 5 (a) Fraction of ions as a function of the number of chains to which they are coordinated. (b) Homopolymer and (c) block copolymer: average based on the instantaneous state of coordination of ions. Insets to the figure shows the fraction of ions that jumped between 1 and 2 chains.

leading to changes in the coordination state of the ions occur only very infrequently; (ii) among the non-integer coordinations, the distribution of the instantaneous fraction of chains coordinated is seen to be more or less uniformly distributed between 1 and 2 chains for BCPs (inset of Fig. 5(c)), whereas the distribution is more biased towards the values near 1 for the case of homopolymers (inset of Fig. 5(b)). Such results are consistent with the discussion underlying Type 3 events above and indicate that instances where ions do transform from being coordinated with single chain to becoming involved with multiple chains occur more often in BCPs relative to HPs.

The above discussion of ion hopping mechanisms pertained to the inter and intrasegmental hops along the backbone of the chain. Interestingly, in all the above five cases, the complexation of anions was rarely observed. In a few cases however, when there existed at least three anions coordinated per lithium cation, the ion motion was influenced by the motion of the complexed anion–cations. Such cases of complexation with multiple anions were not observed in the context of homopolymer melts, and likely arise as a consequence of the stronger coordination between Li and PF_6 ions in the case of BCPs when compared to homopolymer melts (*cf.* discussion corresponding to Fig. 4 in ref. 47).

Overall, the above results provide a detailed description of ion hopping mechanisms in block copolymers relative to homopolymers. The mechanisms underlying ion motions were observed to exhibit similar characteristics in BCPs and HPs. However, as a consequence of the conformational effects arising from microphase separation, specific modes of transport were observed more frequently in BCP systems. Our results also indicated that in the case of block copolymer, the cations prefer to stay complexed with the backbone of the chain rather than engaging with anions.

We note that in previous study on homopolymers[33] a mode of hopping of ions between two chains facilitated by anions was observed. However, such a mechanism was not observed in our work. In addition to the influence of microphase separation, such differences could also be a consequence of (a) slower BCP dynamics in our system; and the (b) non-polarizable forcefields utilized in this study.

3.3 Effects of salt concentration

In this section, we present results characterizing the influence of salt concentration on the mobility of ions and the mechanisms accompanying ion motion in BCPs.

3.3.1 Dynamics of ions and polymers. Fig. 6(a) compares the mean squared displacements of the lithium ions in BCP (overall) with those in pure PEO melts as a function of salt concentration. With increasing salt concentration, it can be observed that the displacement of the ions become smaller, indicating that the dynamics become slower in both block copolymers and homopolymer melts. Interestingly, the mean squared displacements in the BCP system and homopolymer PEO melts are seen to become similar for the highest salt concentrations. The latter results are broadly consistent with experimental observations which have noted that the differences in the conductivities of BCPs and homopolymers become reduced for higher salt concentrations.[27]

As discussed earlier, we were not able to achieve the long time, linear regime for the mean squared displacements, and hence were unable to extract the true ion diffusivities. As an alternate means of comparison of the mobility of the ions, we display the average displacement of the ions at 30 ns (Fig. 6(b)) for both BCP and homopolymer melts at different salt concentrations. From Fig. 6(b), it is clear that the ions move larger displacements in homopolymers compared to BCPs at low salt concentrations, whereas the displacements are comparable at high salt concentrations. Such results indicate that the ion mobility in homopolymer and BCP melts becomes comparable at high salt concentration limits.

To understand the above results, we again invoke the changes in polymer segmental dynamics arising as a consequence of

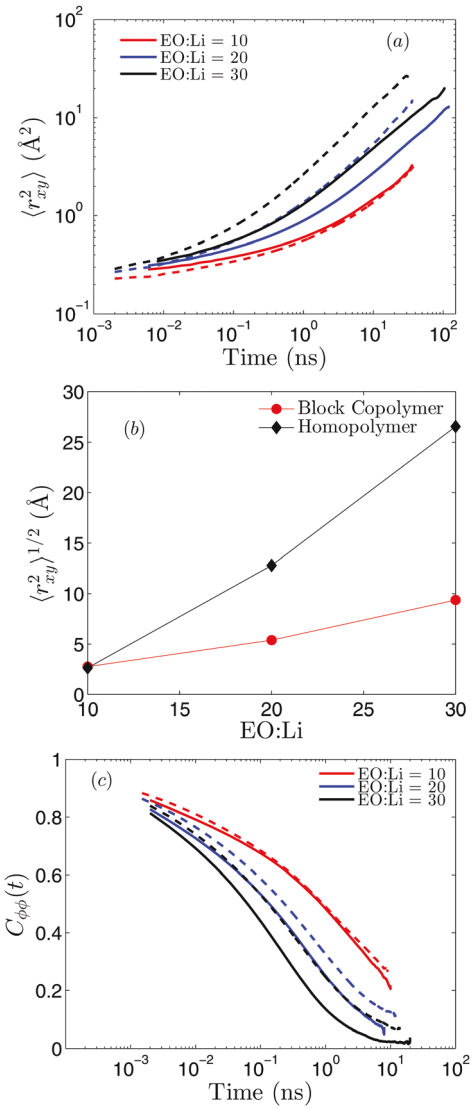

Fig. 6 (a) Mean squared displacements as a function of salt concentration in BCP (overall) and pure homopolymer melt. Solid lines correspond to MSDs of BCP and dotted lines correspond to MSDs of PEO melt. Only the portion beyond the initial ballistic regime is depicted; (b) lithium displacement at 30 ns; (c) dihedral–dihedral autocorrelation function as a function of salt concentration. Solid lines correspond to BCPs and dotted lines correspond to PEO homopolymer melts. Only the portion of the autocorrelation function beyond the initial decay is depicted.

the combined effects of microphase separation and the salt concentrations. In Fig. 6(c), we display the polymer segmental relaxations in BCP (dotted lines) and homopolymers (solid lines) as a function of salt concentration. Therein, it can be seen that with increasing salt concentration, the polymer dynamics indeed becomes slowed in both BCP and homopolymers. Moreover, consistent with the results of Fig. 6(a), for the highest salt concentrations, the relaxation of polymer dynamics is seen to become comparable between the homopolymer and block copolymers. To maintain brevity of the article, in the ESI,† we present results for the salt concentration dependence of the ion residence times (Fig. S5, ESI†). In brief, therein it is seen that with increasing salt concentration, the residence times of the ions with the polymer backbone increases, consistent with the slower polymer and ion dynamics.

To understand the above results, we note that with increase in salt concentrations, a larger number ions are expected to coordinate with the polymer backbone, and lead to more instances where the ions bind simultaneously to multiple polymer chains and act as a "crosslinker". Such effects are expected to manifest in both homopolymers and BCPs and hinder the dynamics of the polymer segments and correspondingly increase the relaxation times.[33,40]

Why do the differences between BCPs and HPs become mitigated at higher salt concentrations? While we do not have a conclusive resolution of this observation, based on earlier work[41,43] we suggest that the dynamical influence of the glassy PS blocks and the microphase separation itself becomes mitigated when the asymmetry in dynamics between the conducting and nonconducting blocks become reduced. As argued above, with increasing salt concentration the dynamics of EO segments are themselves expected to become slower, which reduces the differences in the dynamical characteristics of PS and PEO blocks, which possibly renders the influence of microphase separation less important.

In summary, in this section we presented the effects of salt concentration on ion transport in BCP lamellae. Our results indicate that an increase in the salt concentration results in the reduction of ion mobilities. Such reduction in mobility of ions arise from the reduction in polymer segmental dynamics which in turn is arising from the cross-linking of salt with the polymer backbone. Pertinently, the ion mobilities of BCPs and homopolymers were found to be become comparable at higher salt concentrations.

3.3.2 Mechanisms of ion transport. Ion transport mechanisms were also studied as a function of salt concentration. However, for the range of salt concentrations investigated, we observe that there are no substantial differences in the ion transport mechanisms discussed in Section 3.2. Explicitly, with the change in salt concentration, the five distinct mechanisms that were observed in the context of the EO : Li = 20 : 1 (Section 3.2) were also observed at other concentrations. To maintain brevity, we eschew repeating the underlying features.

Fig. 7(a)–(c) displays the instantaneous fraction of ions coordinated with n number of chains for different salt concentrations. Therein, it can be observed that fraction of ions that are coordinated to no chains increase with increasing salt concentration. Such results indicate that with increasing salt concentration, there is an increased pairing of the cations with the anions, and can be rationalized based on the increase in strength of $LiPF_6$ coordination (and the saturation of polymer backbone sites for coordination of cations) with increasing salt concentration. Accordingly, the ensemble average of the fraction of ions (Fig. 7(d)) also shows an increase in the fraction of ions that are coordinated with no chains with increasing salt concentration. However, the distribution of jumps (insets of Fig. 7(a)–(c)) are observed to be relatively insensitive to salt concentrations.

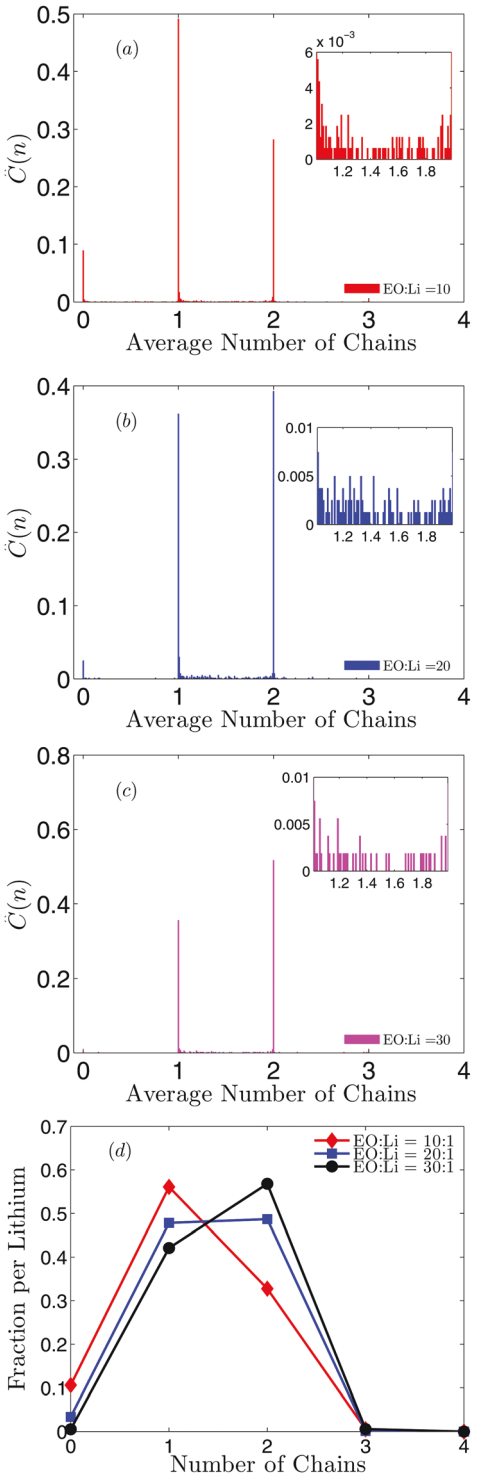

Fig. 7 Fraction of the instantaneous number of chains coordinated for EO : Li = (a) 10 : 1; (b) 20 : 1; (c) 30 : 1. (d) Average fraction of ions coordinated as a function of number of chains for block copolymers.

4 Summary

In summary, a multiscale simulation strategy was employed to understand the dynamical properties of ions in salt doped BCP melts. Specifically, we quantified the ion transport properties in the lamellar phase of block copolymer melts and compared such properties with pure PEO homopolymer melts. Our results indicate that the mean squared displacements for ions were lower in BCP melts compared to their homopolymer counterparts. Correspondingly, the ions are found to have larger residence times near the polymer backbone in BCP melts compared to homopolymer melts. Such results were rationalized based on the slower polymer segmental dynamics in BCP melts compared to homopolymer melts.

Investigations on ion transport mechanism in BCP melts revealed five different mechanisms. While the mechanisms were observed to exhibit similar characteristics in BCPs and HPs, however, as a consequence of the conformational effects arising from microphase separation, a few specific modes of transport were observed more frequently in BCP systems.

Finally, effects of salt concentrations were also studied. It was seen that increasing salt concentration leads to a reduction in the mean squared displacements and an increase in residence times. However, the differences in ion dynamics between BCPs and homopolymers were found to become reduced with increasing salt concentration.

Conflicts of interest

There are no conflicts to declare.

Acknowledgements

VG acknowledges funding in part by grants from the Robert A. Welch Foundation (Grant F1599), the National Science Foundation (DMR-1721512), and to King Abdullah University of Science and Technology (OSR-2016-CRG5-2993-1). Acknowledgment is also made to the Donors of the American Chemical Society Petroleum Research Fund for partial support of this research (56715-ND9). The authors acknowledge the Texas Advanced Computing Center (TACC) for computing resources.

References

1 P. V. Wright, *Br. Polym. J.*, 1975, **7**, 319–327.
2 P. G. Bruce and C. A. Vincent, *J. Chem. Soc., Faraday Trans.*, 1993, **89**, 3187–3203.
3 S. Mogurampelly, O. Borodin and V. Ganesan, *Annu. Rev. Chem. Biomol. Eng.*, 2016, **7**, 349–371.
4 M. Armand, *Solid State Ionics*, 1983, **910**(Part 2), 745–754.
5 M. Armand, *Adv. Mater.*, 1990, **2**, 278–286.
6 P. Cotanda, G. Sudre, M. A. Modestino, X. C. Chen and N. P. Balsara, *Macromolecules*, 2014, **47**, 7540–7547.
7 J. Shi and C. A. Vincent, *Solid State Ionics*, 1993, **60**, 11–17.
8 T. H. Epps, T. S. Bailey, R. Waletzko and F. S. Bates, *Macromolecules*, 2003, **36**, 2873–2881.
9 W.-S. Young, W.-F. Kuan and T. H. Epps, *J. Polym. Sci., Part B: Polym. Phys.*, 2014, **52**, 1–16.
10 R. Yuan, A. A. Teran, I. Gurevitch, S. A. Mullin, N. S. Wanakule and N. P. Balsara, *Macromolecules*, 2013, **46**, 914–921.

11 Y. A. Elabd and M. A. Hickner, *Macromolecules*, 2011, **44**, 1–11.
12 K. M. Abraham, Z. Jiang and B. Carroll, *Chem. Mater.*, 1997, **9**, 1978–1988.
13 M. A. Ratner and D. F. Shriver, *Chem. Rev.*, 1988, **88**, 109–124.
14 G. Mao, M.-L. Saboungi, D. L. Price, Y. S. Badyal and H. E. Fischer, *EPL*, 2001, **54**, 347–353.
15 G. Mao, M.-L. Saboungi, D. L. Price, M. B. Armand and W. S. Howells, *Phys. Rev. Lett.*, 2000, **84**, 5536–5539.
16 M. D. Green, D. Wang, S. T. Hemp, J.-H. Choi, K. I. Winey, J. R. Heflin and T. E. Long, *Polymer*, 2012, **53**, 3677–3686.
17 M. D. Green, J.-H. Choi, K. I. Winey and T. E. Long, *Macromolecules*, 2012, **45**, 4749–4757.
18 S. Zhang, K. H. Lee, J. Sun, C. D. Frisbie and T. P. Lodge, *Macromolecules*, 2011, **44**, 8981–8989.
19 M. T. Irwin, R. J. Hickey, S. Xie, S. So, F. S. Bates and T. P. Lodge, *Macromolecules*, 2016, **49**, 6928–6939.
20 A. Panday, S. Mullin, E. D. Gomez, N. Wanakule, V. L. Chen, A. Hexemer, J. Pople and N. P. Balsara, *Macromolecules*, 2009, **42**, 4632–4637.
21 W.-S. Young and T. H. Epps, *Macromolecules*, 2009, **42**, 2672–2678.
22 W.-S. Young, J. N. L. Albert, A. B. Schantz and T. H. Epps, *Macromolecules*, 2011, **44**, 8116–8123.
23 J.-H. Choi, Y. Ye, Y. A. Elabd and K. I. Winey, *Macromolecules*, 2013, **46**, 5290–5300.
24 M. Singh, O. Odusanya, G. M. Wilmes, H. B. Eitouni, E. D. Gomez, A. J. Patel, V. L. Chen, M. J. Park, P. Fragouli, H. Iatrou, N. Hadjichristidis, D. Cookson and N. P. Balsara, *Macromolecules*, 2007, **40**, 4578–4585.
25 D. Devaux, D. Glé, T. N. T. Phan, D. Gigmes, E. Giroud, M. Deschamps, R. Denoyel and R. Bouchet, *Chem. Mater.*, 2015, **27**, 4682–4692.
26 D. R. Wang, K. H. Wujcik, A. A. Teran and N. P. Balsara, *Macromolecules*, 2015, **48**, 4863–4873.
27 M. Chintapalli, T. N. P. Le, N. R. Venkatesan, N. G. Mackay, A. A. Rojas, J. L. Thelen, X. C. Chen, D. Devaux and N. P. Balsara, *Macromolecules*, 2016, **49**, 1770–1780.
28 S. Sharick, J. Koski, R. A. Riggleman and K. I. Winey, *Macromolecules*, 2016, **49**, 2245–2256.
29 T. H. Epps, T. S. Bailey, H. D. Pham and F. S. Bates, *Chem. Mater.*, 2002, **14**, 1706–1714.
30 A.-V. G. Ruzette, P. P. Soo, D. R. Sadoway and A. M. Mayes, *J. Electrochem. Soc.*, 2001, **148**, A537–A543.
31 L. Xie and G. Farrington, *Solid State Ionics*, 1992, **53**, 1054–1058.
32 C. Catlow and G. Mills, *Electrochim. Acta*, 1995, **40**, 2057–2062.
33 O. Borodin and G. D. Smith, *Macromolecules*, 1998, **31**, 8396–8406.
34 S. Neyertz and D. Brown, *J. Chem. Phys.*, 1996, **104**, 3797–3809.
35 O. Borodin and G. D. Smith, *Macromolecules*, 2000, **33**, 2273–2283.
36 D. Diddens, A. Heuer and O. Borodin, *Macromolecules*, 2010, **43**, 2028–2036.
37 F. Müller-Plathe and W. F. van Gunsteren, *J. Chem. Phys.*, 1995, **103**, 4745–4756.
38 A. Maitra and A. Heuer, *Phys. Rev. Lett.*, 2007, **98**, 227802.
39 A. Aabloo and J. Thomas, *Solid State Ionics*, 2001, **143**, 83–87.
40 O. Borodin and G. D. Smith, *J. Phys. Chem. B*, 2006, **110**, 4971–4977.
41 V. Sethuraman, V. Pryamitsyn and V. Ganesan, *J. Polym. Sci., Part B: Polym. Phys.*, 2016, **54**, 859–864.
42 V. Ganesan, V. Pyramitsyn, C. Bertoni and M. Shah, *ACS Macro Lett.*, 2012, **1**, 513–518.
43 V. Sethuraman and V. Ganesan, *Soft Matter*, 2016, **12**, 7818–7823.
44 G. Milano and F. Müller-Plathe, *J. Phys. Chem. B*, 2005, **109**, 18609–18619.
45 M. Murat, G. S. Grest and K. Kremer, *Macromolecules*, 1999, **32**, 595–609.
46 C. Peter and K. Kremer, *Faraday Discuss.*, 2010, **144**, 9–24.
47 V. Sethuraman, S. Mogurampelly and V. Ganesan, *Macromolecules*, 2017, **50**, 4542–4554.
48 J. M. Stubbs, J. J. Potoff and J. I. Siepmann, *J. Phys. Chem. B*, 2004, **108**, 17596–17605.
49 M. G. Martin and J. I. Siepmann, *J. Phys. Chem. B*, 1998, **102**, 2569–2577.
50 C. D. Wick, M. G. Martin and J. I. Siepmann, *J. Phys. Chem. B*, 2000, **104**, 8008–8016.
51 G. Santangelo, A. Di Matteo, F. Müller-Plathe and G. Milano, *J. Phys. Chem. B*, 2007, **111**, 2765–2773.
52 K. C. Daoulas, M. Muller, J. J. de Pablo, P. F. Nealey and G. D. Smith, *Soft Matter*, 2006, **2**, 573–583.
53 N. A. Kumar and V. Ganesan, *J. Chem. Phys.*, 2012, **136**, 101101.
54 D. Kipp and V. Ganesan, *J. Phys. Chem. B*, 2014, **118**, 4425–4441.
55 D. Kipp, O. Wodo, B. Ganapathysubramanian and V. Ganesan, *ACS Macro Lett.*, 2015, **4**, 266–270.
56 D. Kipp, R. Verduzco and V. Ganesan, *J. Polym. Sci., Part B: Polym. Phys.*, 2016, **54**, 884–895.
57 W. Tschöp, K. Kremer, O. Hahn, J. Batoulis and T. Bürger, *Acta Polym.*, 1998, **49**, 75–79.
58 C. F. Abrams and K. Kremer, *Macromolecules*, 2003, **36**, 260–267.
59 B. Steinmüller, M. Müller, K. R. Hambrecht, G. D. Smith and D. Bedrov, *Macromolecules*, 2012, **45**, 1107–1117.
60 S. Plimpton, *J. Comp. Physiol.*, 1995, **117**, 1–19.
61 I. Leontyev and A. Stuchebrukhov, *Phys. Chem. Chem. Phys.*, 2011, **13**, 2613–2626.
62 O. Borodin, G. D. Smith and R. Douglas, *J. Phys. Chem. B*, 2003, **107**, 6824–6837.
63 J. Rieger, *J. Therm. Anal.*, 1996, **46**, 965–972.
64 N. A. Stolwijk, C. Heddier, M. Reschke, M. Wiencierz, J. Bokeloh and G. Wilde, *Macromolecules*, 2013, **46**, 8580–8588.